Low-Capacitance Cascaded H-Bridge Multilevel StatCom

Ghias Farivar, *Student Member, IEEE*, Christopher David Townsend, *Member, IEEE*, Branislav Hredzak, *Senior Member, IEEE*, Josep Pou, *Senior Member, IEEE*, and Vassilios G. Agelidis, *Fellow, IEEE*

***Abstract*—This paper introduces a cascaded H-bridge multilevel converter (CHB-MC)-based StatCom system that is able to operate with extremely low dc capacitance values. The theoretical limit is calculated for the maximum capacitor voltage ripple, and hence minimum dc capacitance values that can be used in the converter. The proposed low-capacitance StatCom (*LC*-StatCom) is able to operate with large capacitor voltage ripples, which are very close to the calculated theoretical maximum voltage ripple. The maximum voltage stress on the semiconductors in the *LC*-StatCom is lower than in a conventional StatCom system. The variable cluster voltage magnitude in the *LC*-StatCom system drops well below the maximum grid voltage, which allows a fixed maximum voltage on the individual capacitors. It is demonstrated that the proposed *LC*-StatCom has an asymmetric *V–I* characteristic, which is especially suited for operation as a reactive power source within the capacitive region. A high-bandwidth control system is designed for the proposed StatCom to provide control of the capacitor voltages during highly dynamic transient events. The proposed *LC*-StatCom system is experimentally verified on a low-voltage seven-level CHB-MC prototype. The experimental results show successful operation of the system with ripples as high as 90% of the nominal dc voltage. The required energy storage for the *LC*-StatCom system shows significant reduction compared to a conventional StatCom design.**

***Index Terms*—Capacitor voltage filtering, cascaded H-Bridge, statcom, thin dc capacitor.**

I. Introduction

THE cascaded H-bridge multilevel converter (CHB-MC) is a popular choice in many industrial applications due to its modularity, ability to decrease switching loss while maintaining excellent harmonic performance, and the possibility to eliminate the step-up transformer in medium voltage applications [1], [2]. An additional feature that makes this converter suitable for the StatCom application is its linear relationship between level number and component count [2], as opposed to monolithic multilevel converters, where this relationship is quadratic.

Compared to monolithic multilevel converters, the requirement for isolated dc power sources is considered to be one of the main disadvantages [1]. However, in StatCom applications the isolated dc sources are floating capacitors and, therefore, the isolation requirement is easily met. The idea of using a CHB-MC as a StatCom was introduced in [3]. Thereafter, different aspects of this application for CHB-MC have been studied in the technical literature [4]–[24].

The three-phase CHB converter is constructed from three single-phase converters connected via a common star-point. This implies that each phase-leg must buffer the per-phase variations in instantaneous power that occur within each fundamental cycle, which is in contrast to monolithic multilevel converters which have a common dc link. To buffer the energy variations, while still maintaining the necessary capacitor voltage to control the converter current, significant energy storage is required within each CHB phase-leg. This dictates the use of large H-bridge capacitance values, which has the following drawbacks:

1) high direct cost of large dc capacitors;
2) the indirect cost on reliability of the system due to the tendency of electrolytic capacitors to fail before other system components [25], [26];
3) the indirect cost on cell protection due to the very large energy that is dissipated in the event of shoot-through of the dc link;
4) the significant weight and volume of the converter, which can make it difficult to containerise high-power StatComs.

Recently, the high reliability of film capacitors has become a major driving force in replacing electrolytic capacitors in power converters [27]–[30]. However, the relatively low-capacitance values achievable with film capacitors, compared to electrolytic capacitors with the same volume, has limited the application of film capacitors in CHB-MC applications.

In typical CHB converters, the H-bridge capacitance values are chosen to limit variations in capacitor voltages to 10% of the nominal dc voltage [31]. There are two reasons why voltage variation must be limited. The first is that the peak voltage on each capacitor must be limited to avoid destruction of the associated semiconductor devices and to avoid lifetime reduction due to cosmic-ray failure rate implications [32]. The second reason is the lower limit on capacitor voltage variation, which is dictated by the need to maintain sufficient cluster voltage such that effective current control can be maintained throughout the fundamental cycle. Cluster voltage is defined as the sum of H-bridge capacitor voltages in one phase.

The main premise of the proposed approach in this paper is based on the observation that the lower limit on capacitor voltage variation can be significantly lowered when the *V–I* operating characteristic of the converter is somewhat restricted.

Manuscript received December 22, 2015; revised March 5, 2016; accepted April 11, 2016. Date of publication April 21, 2016; date of current version December 9, 2016. Recommended for publication by Associate Editor ZiXin Li.

The authors are with the Australian Energy Research Institute and the School of Electrical Engineering and Telecommunication, University of New South Wales (UNSW Australia), Sydney, N.S.W. 2052, Australia (e-mail: g.farivar@unsw.edu.au; Townsend@ieee.org; b.hredzak@unsw.edu.au; j.pou@unsw.edu.au; vassilios.agelidis@unsw.edu.au).

Color versions of one or more of the figures in this paper are available online at http://ieeexplore.ieee.org.

Digital Object Identifier 10.1109/TPEL.2016.2557351

It is shown that when operating in the capacitive region, the synthesized output voltage waveform has the same phase angle as the capacitor voltage ripple waveform. This implies current control can be maintained even when the cluster voltage reduces to almost zero.

Allowing larger capacitor voltage variations implies the use of significantly lower H-bridge capacitance values. The achieved reduction in the total stored capacitor energy will be shown in this paper. The required restrictions in the *V–I* operating characteristic will also be defined in this paper.

There are two main issues that need to be addressed to operate a CHB-MC with large H-bridge capacitor voltage ripples. First, the bandwidth of the converter control system must be very high to maintain good voltage regulation on the thin-film capacitors. Second, the effect of high-magnitude low-order capacitor voltage harmonics on the control system and grid current needs to be minimized, while simultaneously maintaining high-bandwidth control of the capacitor voltages. This paper develops a control structure capable of achieving these goals within the proposed StatCom concept. The effect of low-order capacitor voltage harmonics on the control system is minimized by using an analytic filtering scheme, which imposes negligible delay. This allows high-bandwidth control within the loop responsible for regulating the cluster voltage. Additionally, a dead-beat controller is utilized in this paper to obtain high-bandwidth current control [33], [34]. Feedforward compensation within the PWM module is also used to mitigate any effect of capacitor voltage ripples on the grid current [35], which would otherwise be introduced from the modulation stage.

In a CHB-MC based StatCom, voltage variation on each H-bridge capacitor mainly manifests as a second-order harmonic component. The ripple magnitude increases when the H-bridge capacitance decreases, which makes filtering of these voltages within the controller more challenging in the LC-StatCom. The cutoff frequency of the typically used low-pass filter for capacitor voltages is reduced while simultaneously the bandwidth of the voltage balance control loop is increased, causing difficulty in maintaining tight regulation of capacitor voltages during transients. In previous CHB-MC StatCom controllers, these two requirements cannot be met simultaneously.

In [36], an analytic filtering scheme is introduced to overcome this challenge. The developed analytic filtering scheme predicts the behavior of ripple on the capacitor voltages and compensates its effect by subtracting the online estimate of the ripple. Therefore, it introduces no delay to the control system. This means the bandwidth of the control system is only limited by the inner loop current controller. However, no attempt has been made within this scheme to minimize the maximum voltage that semiconductors are exposed to. Furthermore, the proposed analytic formula considerably increases the computational burden.

In this paper, to complement the research done in [36], the issue of minimizing the maximum capacitor voltages is addressed. Furthermore, it has been shown previously in [37] (for typical CHB StatComs) that controlling the square of capacitor voltage results in a decoupled and linear cascaded control system. This paper utilizes the same concept to significantly reduce the computational power required to implement the analytic filtering scheme proposed in [36]. The use of complex capacitor voltage filtering is avoided as the ripple on the square of the capacitor voltages is sinusoidal (with a frequency equal to twice that of the grid frequency). Estimation of one sinusoidal waveform per-phase requires much less computational power compared to directly estimating mixed-frequency capacitor voltage signals.

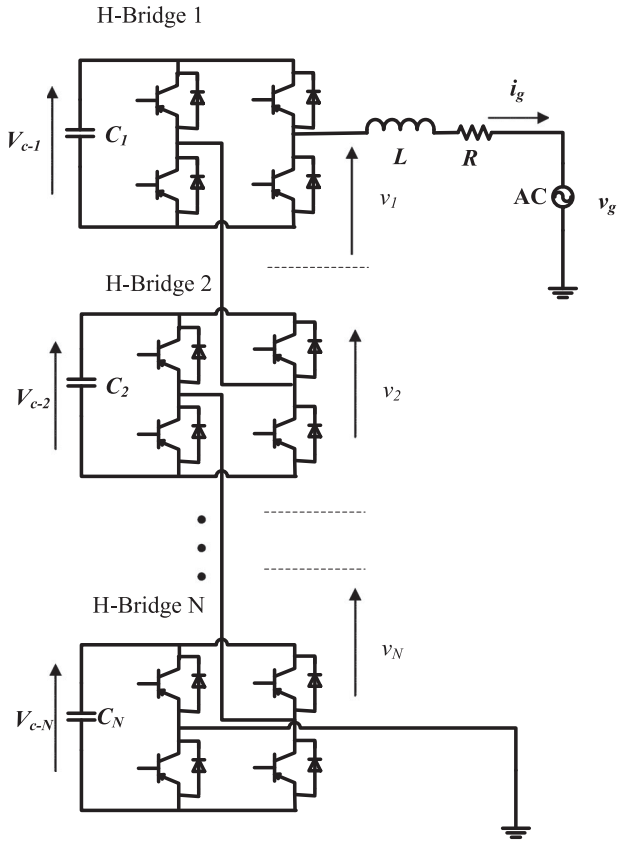

Fig. 1. General single-phase, $(2N + 1)$-level CHB converter-based StatCom system.

The rest of this paper is organized as follows. Section II provides the background on the CHB-MC-based StatCom system. Analysis of the capacitor voltage ripple and the theoretical limits for reactive power exchange is provided in Section III. Experimental results are provided in Section IV. Finally, conclusions from the work are summarized in Section V.

II. Low-Capacitance StatCom (*LC*-StatCom) System

In this section, a model of the CHB converter-based *LC*-StatCom is introduced and an expression for the H-bridge capacitor voltages as a function of the converter current and grid voltage is derived. Fig. 1 shows a single-phase CHB converter *LC*-StatCom. A three-phase configuration is composed of three identical single-phase converters. Therefore, for the rest of this paper, without loss of generality, a single-phase system is considered.

Using Kirchhoff's voltage law on the ac side yields

$$\sum_{j=1}^{N} v_j - v_g - Ri_g - L\frac{di_g}{dt} = 0 \tag{1}$$

where v_j is the ac voltage generated by the *j*th H-bridge ($j\{1,\ldots,N\}$), *L* represents the filter inductor, and *R* is its parasitic series resistance. v_g and i_g are the grid voltage and converter current, respectively.

On the other hand, on the dc side of each H-bridge

$$I_{C-j} + C\frac{dV_{c-j}}{dt} = 0 \tag{2}$$

where *C* represents the capacitance of the capacitors ($C = C_1 = C_2 = \ldots = C_N$) and V_{c-j} is the voltage across the individual capacitors. $I_{C-\mathrm{j}}$ represents the current flowing into the *j*th capacitor. Assuming that the losses are negligible, the input power on the ac side is equal to the output power on the dc side; hence

$$I_{C-j} = \frac{v_j}{V_{c-j}} i_g. \tag{3}$$

Replacing I_{c-j} from (3) in (2) yields

$$\frac{v_j}{V_{c-j}} i_g + C\frac{dV_{c-j}}{dt} = 0. \tag{4}$$

Equations (1) and (4) are the core equations that model the behavior of the CHB converter.

An expression for the capacitor voltages can be derived by assuming cluster voltage is distributed evenly between submodules and solving the resulting differential equation from (4) as follows:

$$\frac{CV_{c-j}^2(t)}{2} = E_j(t_0) + \int_{t_0}^{t} v_j i_g dt \tag{5}$$

where E_j represents the energy stored in the jth capacitor at $t = t_0$. Replacing $v_j = V_{(j)\sin}(\omega t + \alpha_{v-j})$ and $i_g = I_{(g)\sin}(\omega t + \alpha_i)$ in (5), which implies harmonics in both converter current and grid voltage are neglected, then V_{c-j} can be found as follows:

$$V_{c-j}(t) = \sqrt{\begin{array}{l} V_{c-j}^2(t_0) + \frac{V_j I_g}{C} \\ \int_{t_0}^{t} \left[\cos\left(\alpha_{v-j} - \alpha_i\right) - \cos\left(2\omega t + \alpha_{v-j} + \alpha_i\right)\right] dt \end{array}} \tag{6}$$

where ω is the angular frequency of the grid, V_j and α_{v-j} are the peak value and phase angle of v_j, I_g, and α_i represent the peak value and phase angle of the converter current, respectively.

An additional assumption is that the converter current is purely reactive

$$\alpha_i = \alpha_{v-j} \pm \frac{\pi}{2}. \tag{7}$$

Replacing (7) in (6) yields

$$V_{c-j}(t) = \sqrt{\begin{array}{l} V_{c-j}^2(t_0) \pm \frac{V_j I_g}{2\omega C}\left[\cos\left(2\omega t_0 + 2\alpha_{v-j}\right)\right. \\ \left. - \cos\left(2\omega t + 2\alpha_{v-j}\right)\right] \end{array}}. \tag{8}$$

The expression for the capacitor voltage shown in (8) will be used in the next section to design a feedforward ripple compensator for the control system.

III. Control System

The *LC*-StatCom control system is shown in Fig. 2, which comprises three sections, namely: 1) cluster voltage controller, which is responsible for regulating cluster voltage by controlling the active power flow; 2) converter current controller; and 3) individual capacitors' voltage controller that is in charge of evenly distributing cluster voltage between submodules.

The individual capacitor voltage controllers use a separate PI controller to inject small ac voltage components, Δv, in phase with the converter current to balance the capacitor voltages. The total injected components cancel each other out over the phase-leg to ensure no interference with outer control loops [37].

The current controller is based on a popular dead-beat current controller often used in variable speed drive applications [33], [34] to provide excellent dynamic current tracking performance. The dead-beat current controller uses a discretized version of (1) to calculate the appropriate voltage reference, as follows:

$$v_{\mathrm{ref}}^{k+1} = v_g^k + Ri_g^k + Lf_s\left(i_{g-\mathrm{ref}}^{k+1} - i_g^k\right). \tag{9}$$

In (9), v_{ref} represents the total ac voltage reference of the converter, $i_{g-\mathrm{ref}}$ is the converter current reference value, and f_s is the sampling frequency. Superscripts k and $k+1$ indicate the quantity values at present and future instances, respectively. The input reference signal to the current controller, $i_{g-\mathrm{ref}}$, is composed of both active and reactive components. The active current reference $I_{d-\mathrm{ref}}$ is generated by the cluster capacitor voltage controller, and the reactive current reference $I_{q-\mathrm{ref}}$ defines the converter's reactive current.

The cluster voltage controller uses the square of the sum of capacitor voltages to fulfill the decoupling condition with the individual voltage controllers [37]. The individual voltage controller balances the capacitor voltages by exchanging energy between the H-bridges in one phase, where the energy in each capacitor is proportional to the square of its voltage.

Therefore, the individual controller takes care of internal energy balance and the cluster voltage controller needs to act only when the total energy in the capacitors of a phase is not at the reference value. Hence, since both controllers deal with energy in the capacitors they do not interact with each other. As an example, for a simple case of a five-level converter, if the cluster voltage controller regulates the total energy in the capacitors to a value *2E*, then in the unbalanced condition where the energy in the first and second capacitors is $E_1 = E + dE$ and $E_2 = E - dE$, respectively, the action of the individual voltage controller in transferring dE from the first to the second capacitor will not require any action from the cluster voltage controller, which is the desired decoupled situation. This happens provided the cluster controller regulates the total energy in the phase, but not the total voltage. If the cluster controller targeted the regulation of the total voltage of the phase instead, it would try to take energy out of the leg in this example without being necessary and, hence, would be interacting with the internal controller.

Using the square of the voltages also linearizes the cluster voltage controller [37], which is important in the *LC*-StatCom system as will be discussed in the following analysis. The

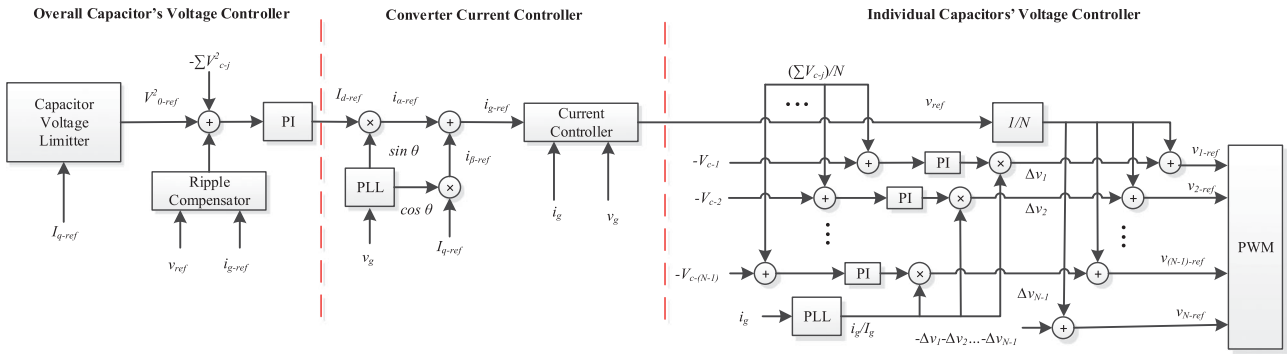

Fig. 2. Proposed LC-StatCom control system composed of three sub-modules: (i) cluster voltage controller, (ii) current controller, and (iii) voltage balancing (individual capacitors' voltage controller).

capacitor voltage reference in this system is not constant and varies throughout a wide range. Furthermore, the use of complex feedforward ripple compensation can be avoided because the ripple on the square of the voltages is sinusoidal

$$\sum_{j=1}^{N} V_{c-j}^2(t) = V_0^2 \pm \frac{VI_g}{2\omega C}\cos(2\omega t + 2\alpha_v). \tag{10}$$

In (10), V is the peak value of the generated ac voltage by the inverter and α_v is its angle. V_0^2 is the square of the dc component in the cluster voltage, which is controlled by the cluster voltage controller. In this single-phase system, the ripple compensator block subtracts the oscillating part by estimating the ripple

$$\pm \frac{V_{\text{ref}} I_{g-\text{ref}}}{2\omega C}\cos(2\omega t + 2\alpha_v). \tag{11}$$

The estimated ripple is subtracted from the measured cluster voltage.

Remark: For three-phase systems, the control loop responsible for regulating the sum of all the capacitor voltages inside the converter will not be affected by the sinusoidal ripple component as it will be canceled out between the phases. In the three-phase system, the estimation of the ripple can instead be used in the control loop responsible for distributing capacitor voltage evenly between the phases.

In the proposed *LC*-StatCom system, $V_{0-\text{ref}}^2$ is a function of the reactive current reference. The reason for having a variable capacitor voltage reference is to keep the maximum allowed voltage on the capacitors constant. Hence, $V_{0-\text{ref}}^2$ is generated by the capacitor voltage limiter (CVL) block to limit the maximum voltage on the capacitors. The CVL block in this paper has two operating modes, which are introduced in the following.

A. Normal Operating Mode

In the normal operating mode, the system operates with a fixed maximum dc voltage. From (10), the total maximum voltage on the capacitors can be approximated as

$$V_{\text{dc}-\max} = N\sqrt{\frac{V_{0-\text{ref}}^2}{N} + \frac{(V_g + X_L I_{q-\text{ref}})I_{q-\text{ref}}}{2\omega NC}} \tag{12}$$

were X_L is the reactance of L. From (12), in order to have a constant $V_{(\text{dc}-\max)}$, $V_{(0-\text{ref})}^2$ needs to be a function of $I_{q-\text{ref}}$, which is defined as follows:

$$V_{0-\text{ref}}^2 = \frac{(aV_{\text{gn}})^2}{N} - \frac{(V_g + X_L I_{q-\text{ref}})I_{q-\text{ref}}}{2\omega C}, \quad (I_{q-\text{ref}} \le I_{\text{qn}}). \tag{13}$$

In (13), subscript *n* indicates the nominal value of a quantity, a is a constant, and aV_{gn} represents the maximum limit for the cluster capacitors' voltage. In practice, the maximum dc voltage needs to be higher than the grid voltage to compensate for the voltage drop across the filter inductor. Therefore, the parameter a needs to be larger than one $(a > 1)$.

The *LC*-StatCom control system can keep $V_{\text{dc}-\max}$ fixed at aV_{gn} for all values of $I_{q-\text{ref}} < I_{\text{qn}}$. At full load, the minimum instantaneous value of the cluster voltage $V_{(\text{dc}-\min)}$ hits its minimum allowed value.

B. Extended Operating Mode

Converters are often thermally rated for short-term higher-power operation. It is suggested here that for a limited time the *LC*-StatCom can provide currents higher than the nominal current by temporarily increasing $V_{\text{dc}-\max}$. The temporary increase would utilize the margin between peak capacitor voltage and maximum reverse blocking voltage of the semiconductors, typically included to minimize cosmic ray failure rates of semiconductors [38]–[40]. As the increase is temporary, the failure rate probabilities will not be greatly impacted.

In this operating mode, the CVL block will maintain the lower limit of the capacitor voltages while allowing $V_{\text{dc}-\max}$ to exceed aV_{gn}. From (10), the total minimum voltage on the capacitors can be approximated as

$$V_{\text{dc}-\min} = N\sqrt{\frac{V_0^2}{N} - \frac{(V_g + X_L I_{q-\text{ref}})I_{q-\text{ref}}}{2\omega NC}}. \tag{14}$$

From (14), in order to have a constant $V_{\text{dc}-\min}$ for different values of $I_{q-\text{ref}}$, $V_{0-\text{ref}}^2$ needs to be calculated as follows:

$$V_{0-\text{ref}}^2 = \frac{(bV_{\text{gn}})^2}{N} + \frac{(V_g + X_L I_{q-\text{ref}})I_{q-\text{ref}}}{2\omega C}, \quad (I_{q-\text{ref}} \ge I_{\text{qn}}) \tag{15}$$

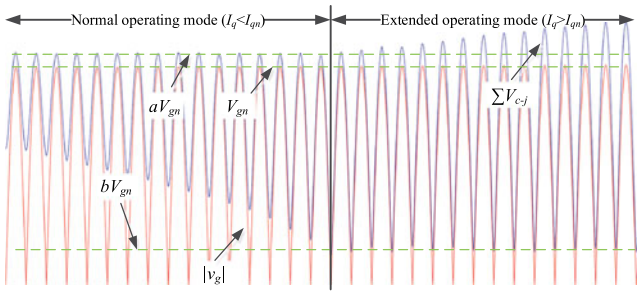

Fig. 3. Illustration of the two operating modes. The reactive power increases linearly as a function of time to illustrate the regulated capacitor voltages in the different regions.

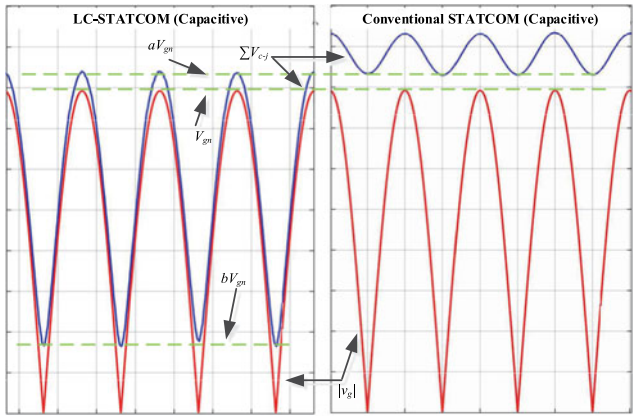

Fig. 4. Comparison between operation of (a) *LC*-StatCom system and (b) conventional StatCom system.

where b is a constant $(0 < b < 1)$ and $bV_{\rm gn}$ represents the cluster voltage lower limit. In Fig. 3, the two operating modes are illustrated.

The nominal current of the converter $I_{\rm qn}$ is the boundary where the operation mode changes. Therefore, from (13) and (15), $I_{\rm qn}$ can be calculated as follows:

$$I_{\rm qn} = \frac{a^2 - b^2}{N} \frac{\omega C V_{\rm gn}}{1 + X_{L(\rm p.u.)}} \tag{16}$$

in which $X_{L(p.u)}$ represents the per-unit value of the filter reactance.

In the following, a conventional StatCom system [31], [36], [37] is considered to facilitate comparison with the *LC*-StatCom system in Section IV. In a conventional StatCom system, the cluster voltage is typically higher than $aV_{\rm gn}$ at all times. Therefore, the minimum fixed dc voltage reference $V_{\rm dc-ref}$ is

$$V_{\rm dc-ref} = aV_{\rm gn} + \frac{\Delta V_{\rm dc}}{2}. \tag{17}$$

In (17), $\Delta V_{\rm dc}$ represents the maximum ripple on the capacitor voltages, which from (10) can be approximated as

$$\Delta V_{\rm dc} = \frac{N I_{\rm qn} V}{2\omega C_c V_{\rm dc}} \tag{18}$$

where C_c represents the capacitance of the capacitors in the conventional StatCom system. The minimum value for C_c is then calculated from the following equation to keep the capacitor voltage ripple component less than 10% of $V_{\rm dc-ref}$:

$$C_c = \frac{0.9 N I_{\rm qn}(V_{\rm gn} + X_L I_{\rm qn})}{0.2\omega(aV_{\rm gn})^2}. \tag{19}$$

With 10% ripple component, the maximum dc voltage for this system is approximately $1.1\, aV_{\rm gn}$.

IV. *LC*-StatCom *I–V* Characteristic

A conventional StatCom system has the capability to provide symmetrical capacitive and inductive reactive currents (neglecting the voltage drop across X_L). In such a system, the minimum cluster voltage for each phase always remains higher than V_g. Therefore, by increasing the capacitor voltage ripple, $V_{\rm dc-max}$ would otherwise become larger. Hence, larger capacitors are needed to avoid this unwanted increase in voltage variation.

The *LC*-StatCom system is able to keep $V_{\rm dc-max}$ constant, which allows operation under increased low-frequency ripple. Therefore, the *LC*-StatCom system requires smaller dc capacitors to deliver the same reactive current compared to the conventional StatCom. In fact, $V_{\rm dc-max}$ in the *LC*-StatCom system, when operated at its theoretical limit, is equal to $V_{\rm dc-min}$ of a conventional StatCom system, as shown in Fig. 4. Therefore, the voltage stress on semiconductors is also lower in the LC-StatCom system.

To achieve these benefits, the *LC*-StatCom system sacrifices symmetrical inductive and capacitive compensation capability, as it is not possible to operate the converter within part of the inductive region. In the capacitive region, the ripple on the capacitor voltages is in phase with the absolute value of the fundamental converter output voltage and grid voltage $(|v_g| = |V_g \sin(\omega t + \alpha_v)|)$, as can be seen from (8). Therefore, the *LC*-StatCom control system is able to reduce the average cluster voltage $V_{\rm dc-avg}$ to values lower than $V_{\rm g}$ in order to keep $V_{\rm dc-max}$ above its lowest allowed value, $bV_{\rm gn}$. This is not the case in the inductive region, where the capacitor voltage ripple and output converter voltage waveforms are of opposite phase angle.

The operational principals of the conventional StatCom and *LC*-StatCom systems are demonstrated in Fig. 4. In this figure, the advantage of the *LC*-StatCom system over the conventional StatCom system can be easily seen. The figure shows that the *LC*-StatCom not only operates with higher ripple on each capacitor voltage, it also reduces peak capacitor voltage and, hence, voltage stress on each semiconductor.

The *I–V* characteristic of the *LC*-StatCom is derived in the following analysis. Henceforth, to simplify the equations, the voltage drop on X_L is neglected and balanced capacitor voltages are assumed. The analysis is performed for the theoretical limit of operation, where $a = 1$ and $b = 0$.

The *LC*-StatCom system can work at a given operating point if the instantaneous cluster voltage is higher than the instantaneous reference voltage (absolute value) for the entire period:

$$NV_c(t) \geq |v_g|. \tag{20}$$

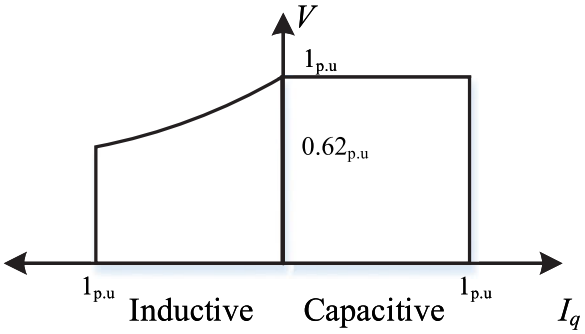

Fig. 5. *I–V* characteristics of the proposed *LC*-StatCom system.

After squaring each side, (20) can be rewritten as

$$NV_c^2(t) \geq \frac{v_g^2}{N}. \tag{21}$$

Assuming the limit case, where $a = 1$ and $b = 0$, from (10) and (13), (21) can be rewritten for the capacitive region as

$$\frac{V_{\rm gn}^2}{N} - \frac{V_g I_q}{2\omega C}[1 + \cos(\theta)] \geq \frac{V_g^2}{2N}[1 - \cos(\theta)] \tag{22}$$

where $\theta = 2\omega t + \alpha_v$. The condition in (22) is valid for any $0 \leq V_g < V_{\rm gn}$ and $0 \leq I_q < I_{\rm qn}$ if it is valid for the worst case (nominal operating condition), where $V_g = V_{\rm gn}$ and $I_q = I_{\rm qn}$. At nominal operating condition, (22) can be rewritten as

$$\left(\frac{V_{\rm gn}}{N} - \frac{I_{\rm qn}}{\omega C}\right)[1 + \cos(\theta)] \geq 0. \tag{23}$$

For the limit case ($a = 1$, $b = 0$, and $X_{(p.u.)} = 0$), from (16) $NI_{\rm qn} = \omega C V_{\rm gn}$. Hence, (23) is valid for the whole period $(0 < \theta \leq 2\pi)$. Consequently, the *I–V* characteristic of the *LC*-StatCom system is equal to the conventional StatCom system $(0 \leq V_g \leq V_{\rm gn},\ 0 \leq I_q \leq I_{\rm qn})$ for the capacitive region.

In the inductive region on the other hand, the following inequality must be satisfied:

$$\frac{V_{\rm gn}^2}{N} - \frac{V_g I_q}{2\omega C}[1 - \cos(\theta)] \geq \frac{V_g^2}{2N}[1 - \cos(\theta)]. \tag{24}$$

The relation between V_g and I_q to define the operating region is determined by replacing $\theta = 3\pi/2$ in (24), resulting in

$$I_q \leq \frac{V_{\rm gn}^2 - V_g^2}{NV_g}\omega C, \quad (0 \leq V_g \leq V_{\rm gn}). \tag{25}$$

By analyzing the inequality in (25), it can be seen that as V_g approaches one, $I_{\rm q}$ approaches zero, while below $V_g \approx 0.62\,V_{\rm gn}$ there is no extra limitation on I_q. The inductive operating region can be described by

$$\begin{aligned} 0 < \ & I_q \leq \frac{V_{\rm gn}^2 - V_g^2}{NV_g}\omega C, \quad (0.62V_{\rm gn} \leq V_g \leq V_{\rm gn}) \\ 0 < \ & I_q \leq I_{\rm qn}, \quad (0 \leq V_g < 0.62V_{\rm gn}). \end{aligned} \tag{26}$$

Therefore, the normalized operating region of the proposed *LC*-StatCom is defined as follows, which is also depicted in Fig. 5.

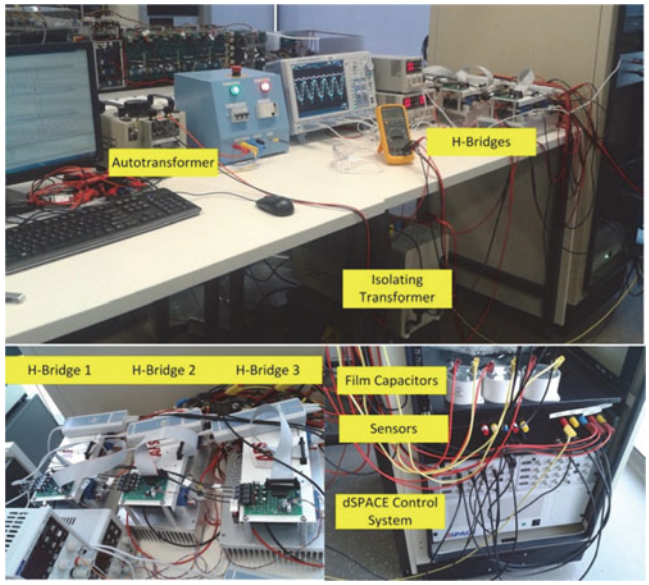

Fig. 6. Experimental setup of a single-phase, seven-level CHB converter LC-StatCom.

TABLE I
PARAMETERS OF THE EXPERIMENTAL *LC*-STATCOM

Symbol	Quantity	Values
$V_{\rm gn-rms}$	Grid voltage rms value	110 V
C	DC capacitor	260 μF
L	Filter inductor	5 mH
f_s	Switching frequency (per H-bridge)	2 kHz
A	Parameter to define maximum capacitors' voltage	1.1
B	Parameter to define minimum capacitors' voltage	0.35
f_g	Grid frequency	50 Hz
S	Converter nominal power	350 VA
R	Filter inductor series resistance	0.5 Ω
w_v	Bandwidth of the voltage controller	300 rad/s
N	Number of H-bridges	3

Capacitive

$$(0 \leq I_{q(\rm p.u.)} \leq 1), \quad (0 \leq V_{g(\rm p.u.)} \leq 1). \tag{27}$$

Inductive

$$\begin{aligned} 0 < \ & I_{q(\rm p.u.)} \leq \frac{1}{V_{g(\rm p.u.)}} - V_{g(\rm p.u.)}, \quad (0.62 \leq V_{g(\rm p.u.)} \leq 1) \\ 0 < \ & I_{q(\rm p.u.)} \leq 1, \quad (0 \leq V_{g(\rm p.u.)} < 0.62). \end{aligned} \tag{28}$$

V. EXPERIMENTAL RESULTS

To experimentally verify the proposed *LC*-StatCom system, a single-phase seven-level CHB converter was constructed. The photograph of the experimental setup is shown in Fig. 6, which parameters are given in Table I. The 240-V grid voltage was reduced to 110 V and isolated from the grid using a step-down transformer. Three POWEREX PP75B060 single-phase H-bridge converters were connected in series to form the seven-level CHB converter. Phase-shifted PWM was implemented using a DS5203 FPGA module. The PWM signals are transferred

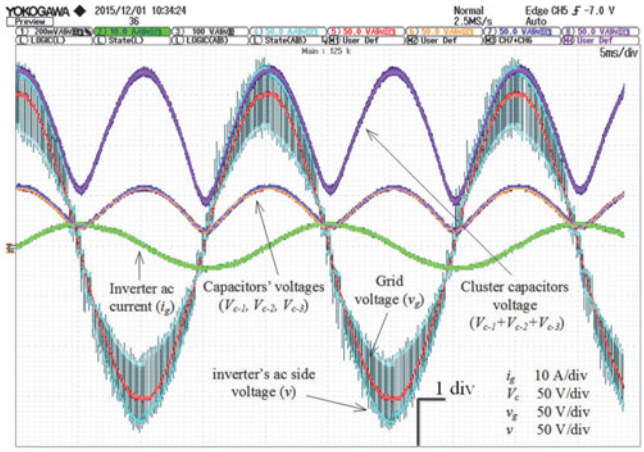

Fig. 7. Operation of the *LC*-StatCom system, when delivering its nominal capacitive current.

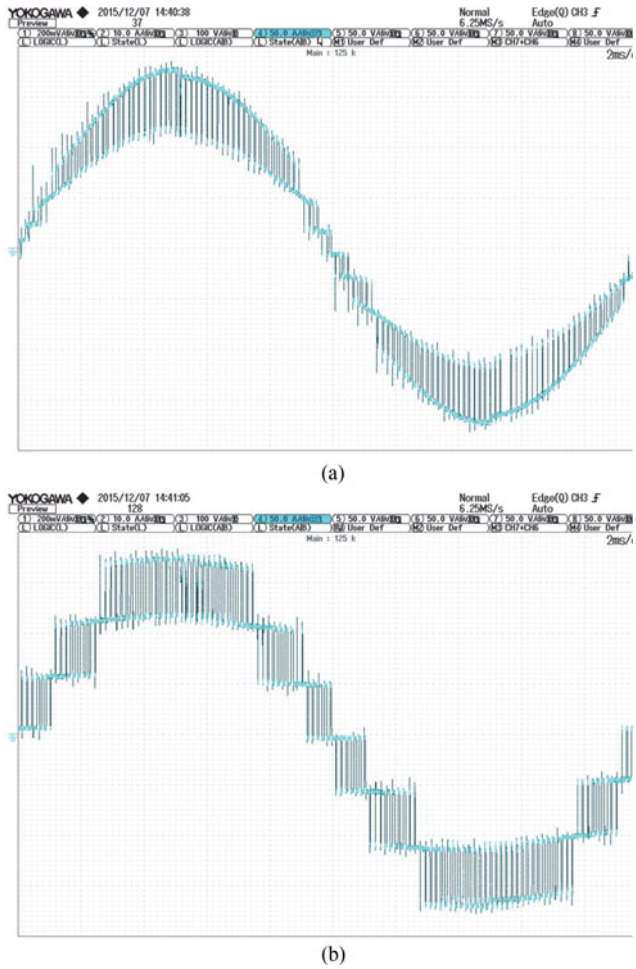

Fig. 8. Synthesized ac voltage: (a) *LC*-StatCom and (b) conventional StatCom.

to the converter driver board by optical link for galvanic isolation. The feedback signals are routed back to the processor using a DS2004 ADC module. All other control systems were implemented using the dSPACE DS1006 processor board.

Stable operation of the proposed *LC*-StatCom system when delivering full capacitive load is shown in Fig. 7. In Fig. 8,

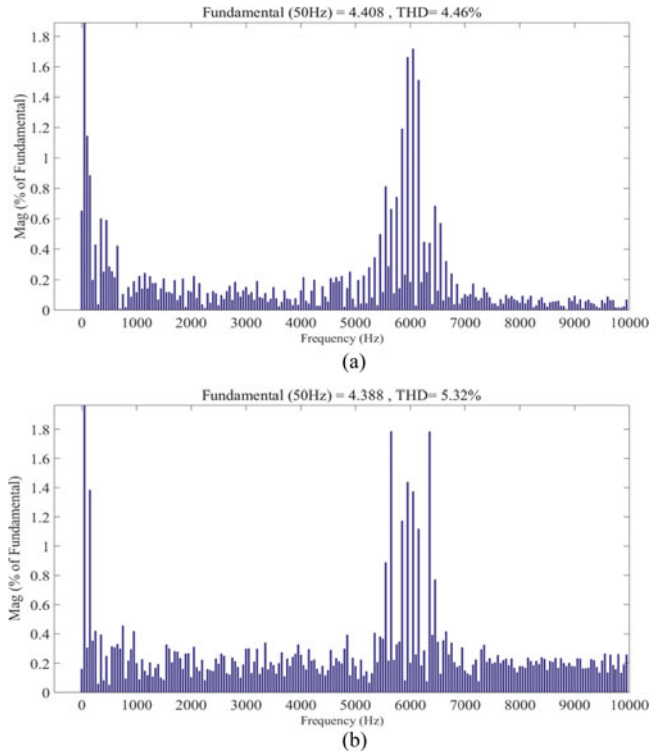

Fig. 9. Harmonics spectrum of the converter current supplied by (a) proposed *LC*-StatCom system and (b) conventional StatCom system.

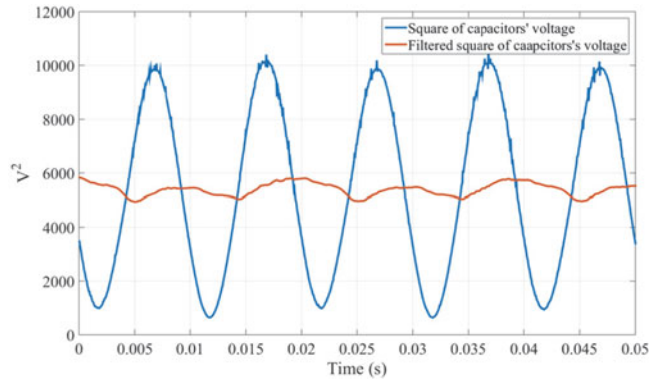

Fig. 10. Filtered and unfiltered square of the capacitors' voltage when the converter is delivering full load capacitive current.

the ac voltage generated by the *LC*-StatCom system is shown and compared to the conventional StatCom system. The results demonstrate a better utilization of the voltage levels within the *LC*-StatCom, due to the converter operating at a more optimal modulation index throughout the fundamental cycle. Hence, the *LC*-StatCom has better current quality than the conventional StatCom system as shown in Fig. 9. Effectiveness of the analytic feedforward filtering technique in removing the second-order component from the square of the capacitor voltages, is shown in Fig. 10.

The next experiment studies operation under step reactive power change, where the reactive current reference is changed from 2 to 4 A at t_0. As it can be seen in Fig. 11, the reactive

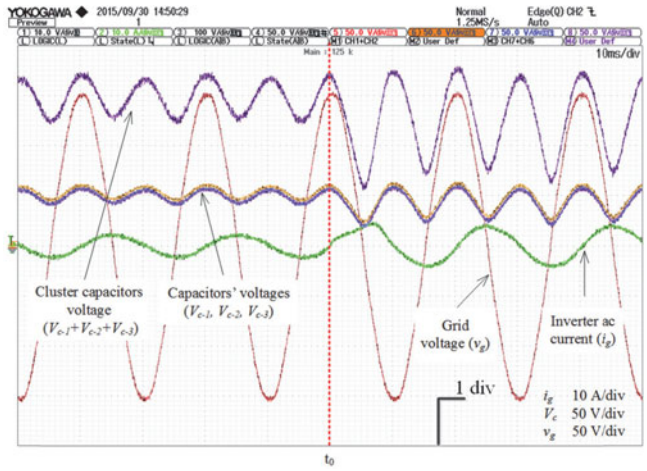

Fig. 11. Operation of the *LC*-StatCom system under step reactive current reference change from 2- to 4-A capacitive at $t = t_0$.

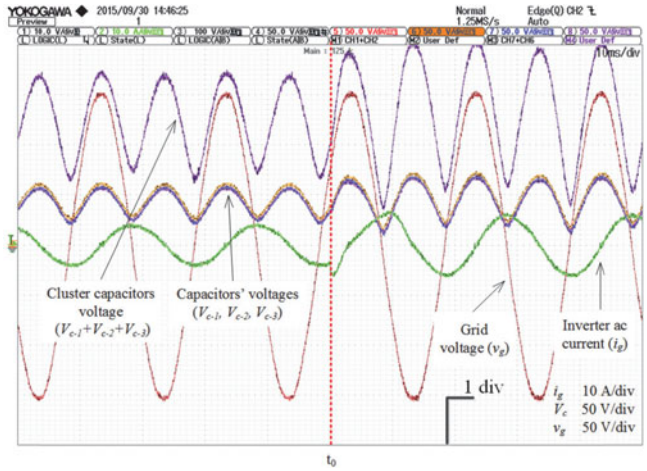

Fig. 12. Transition of the *LC*-StatCom system from normal to extended control mode (step change from 4- to 6-A capacitive at $t = t_0$).

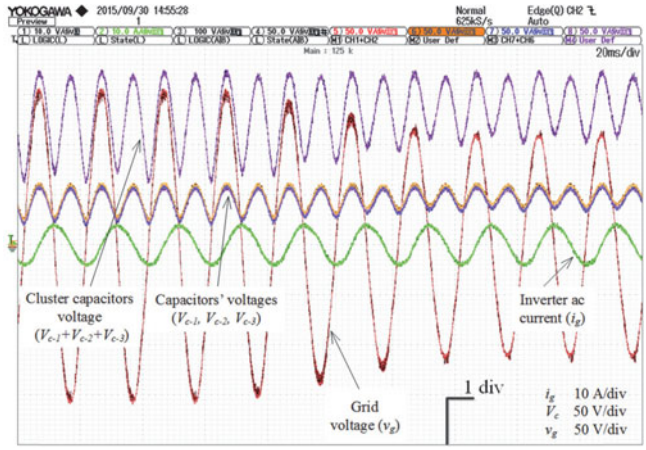

Fig. 13. Operation of the *LC*-StatCom system under varying grid voltage.

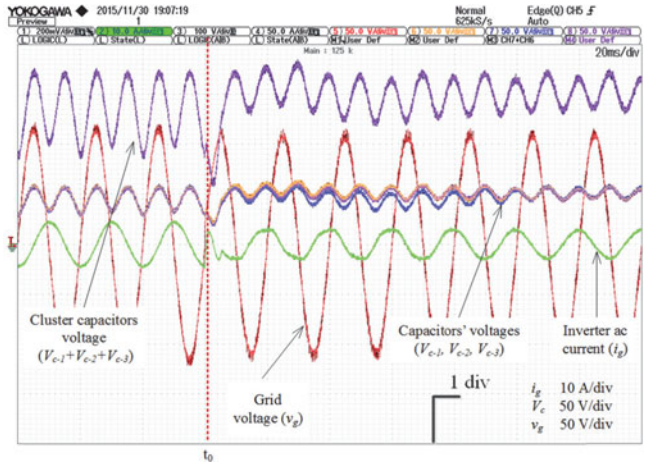

Fig. 14. Operation of the *LC*-StatCom under step change in the reactive current reference from capacitive to inductive at $t = t_0$.

power takes approximately half a cycle to settle to its reference value. This half-a-cycle delay is caused by distorted capacitor voltages during this time. The controller first tries to regulate the capacitor voltages to their reference value, and only then supply the requested reactive current. In a *LC*-StatCom system control of the capacitor voltages must be prioritized during transient events due to the lower "inertia" of the system due to reduced capacitor sizes.

In Fig. 12, a transition from normal to extended control modes is studied. In this case, the reactive power reference transitions from 4 to 6 A at t_0. The control system gives priority to maintain the minimum voltage on the capacitors, and hence, the maximum voltage on the capacitors increases. A smooth transition between the two operating modes can be observed in this figure.

Operation under grid voltage fluctuation is demonstrated in Fig. 13. As can be seen, the *LC*-StatCom's operation was not affected by the transient on the grid voltage. The control system was able to supply the rated current and keep the capacitor voltages below the maximum limit.

To test operation of the proposed *LC*-StatCom system in the inductive region, the grid voltage is reduced to 80 V. Fig. 14 shows the results when the *LC*-StatCom system was initially delivering the rated capacitive current before a step change to 3-A inductive current. The results demonstrate the capability of the *LC*-StatCom system to regulate the maximum capacitor voltages in both inductive and capacitive operating regions. Furthermore, stable operation of the system when moving from inductive to capacitive region can be seen in Fig. 14. In this experiment, there is some distortion in the current right after the transition. This current distortion is produced because the capacitor voltages initially are too low for operation in the inductive region. Therefore, the controller priotizes regulating the capacitor voltages over synthesizing the reactive current reference, which causes some short transients in the converter current.

Fig. 15 shows the results for the case where the step change of the reactive power occurs in the inductive operating region. Here, the reactive current reference is changed from 3- to 2-A inductive at $t = t_0$. As it can be seen, similar to the reactive current step change in the capacitive region, the converter

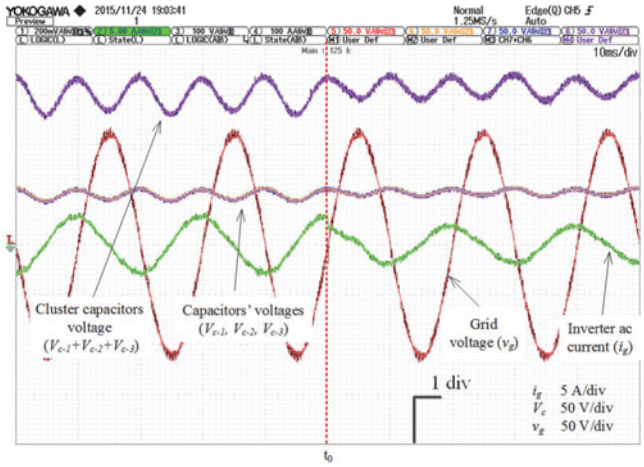

Fig. 15. Operation of the *LC*-StatCom under step change in the reactive current reference from 3- to 2-A inductive at $t = t_0$.

TABLE II
COMPARISON BETWEEN CONVENTIONAL STATCOM WITH DIFFERENT CAPACITOR VOLTAGE RIPPLE DESIGNS AND THE PROPOSED CHB LC-STATCOM

Conventional StatCom parameters			Achieved gains using LC-StatCom	
Capacitor voltage ripple percentage (%)	Maximum dc voltage (V)	Required capacitance per H-bridge cell (mF)	Reduction in maximum dc voltage (%)	Reduction in stored capacitor energy (%)
1	172.8310	11.8	0.9901	97.8447
2	174.5422	5.8	1.9608	95.7308
3	176.2534	3.9	2.9126	93.6560
4	177.9646	2.9	3.8462	91.6184
5	179.6758	2.3	4.7619	89.6159
6	181.3870	1.9	5.6604	87.6467
7	183.0982	1.6	6.5421	85.7090
8	184.8094	1.4	7.4074	83.8010
9	186.5206	1.2	8.2569	81.9212
10	188.2318	1.1	9.0909	80.0678

maintains the maximum value of the capacitor voltages during this transition.

From (19), a conventional StatCom system would require 1-mF capacitors to operate with the same nominal power as the presented experimental *LC*-StatCom system. The maximum dc voltage of the conventional StatCom System would be approximately 188 V compared to 171 V in the *LC*-StatCom. Therefore, the *LC*-StatCom system offers an approximately 80% reduction in the maximum stored capacitor energy compared to a conventional StatCom. In Table II, the proposed *LC*-StatCom is compared to different designs of conventional seven-level StatCom systems with a lower voltage ripple component. The capacitor values in the conventional StatCom designs are selected to produce the desired ripple magnitude at full load (350 VA). The minimum voltage on the dc capacitors of the conventional StatCom systems is 10% higher than the grid voltage amplitude and it is equal to the maximum dc voltage in the *LC*-StatCom system, as shown in Fig 4. As observed in Table II, the capacitance reduction with the proposed *LC*-StatCom is very significant.

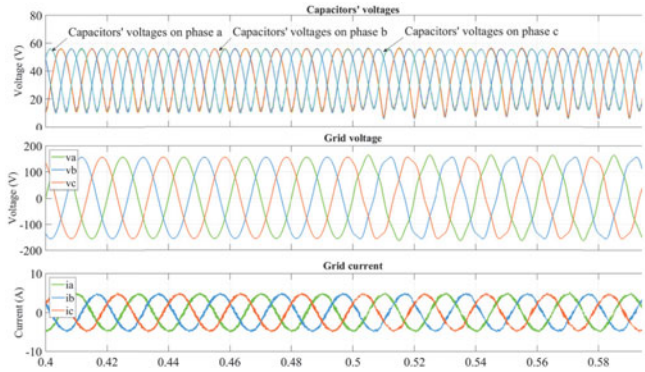

Fig. 16. Operation of the *LC*-StatCom when 5% fifth-order harmonic is added to the grid voltage at $t = 0.5$ s.

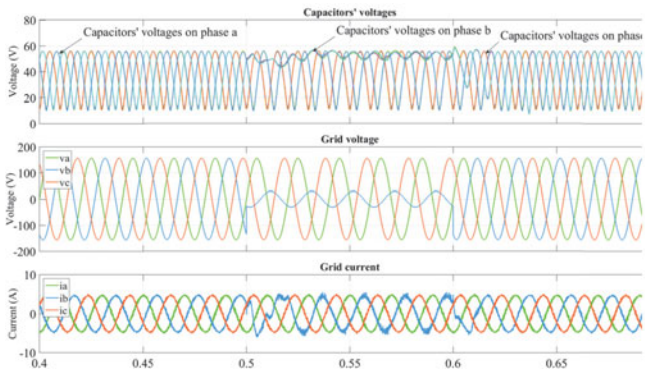

Fig. 17. Operation of the *LC*-StatCom when the grid voltage on phase b, v_b, drops to 0.2 p.u. for five cycles at $t = 0.5$ s.

VI. COMPLIMENTARY SIMULATIONS

In this section, additional simulation results are provided to demonstrate the operation of a three-phase star-connected *LC*-StatCom system under grid voltage abnormalities. The parameters of the simulated system for each phase are shown in Table I. The system is simulated in the MATLAB/Simulink environment.

The simulation result for the case when 5% of fifth harmonic content is added to the grid voltage at $t = 0.5$ s is shown in Fig 16. The result demonstrates stable operation during this test. The capacitor voltages on each phase remain balanced and reactive current supply was not interrupted.

Capability of the *LC*-StatCom system to operate under sudden grid voltage variation and voltage imbalance is shown in Fig. 17. In this case, at $t = 0.5$ s the phase b voltage drops to 0.2 p.u. and after one cycle it returns to 1 p.u. The *LC*-StatCom was able to supply its nominal current even when the grid voltage is heavily unbalanced. The maximum capacitor voltage was maintained on each of the phases. Similar to the experimental results, while the capacitors voltages are temporarily distorted the current does not follow the required reactive reference.

VII. CONCLUSION

A new low-capacitance CHB-MC-based StatCom system has been introduced in this paper. Capacitor voltage ripples in the

LC-StatCom system are increased to facilitate significant capacitance reduction. Simultaneously, the proposed high-bandwidth control structure ensures balanced capacitor voltages during highly dynamic transient events. Hence, as opposed to conventional StatCom systems, utilising large capacitor voltage ripple benefits the overall system size and cost. However, limited inductive capability makes the *I–V* characteristic of the *LC*-StatCom asymmetric. Experimental results on a single-phase seven-level CHB converter have confirmed effective operation of the proposed *LC*-StatCom system under different operational scenarios. It is shown that the *LC*-StatCom system offers better current THD, lower maximum capacitor voltage, and an approximately 80% reduction in the required energy storage capacity when compared to a conventional StatCom system. The proposed *LC*-StatCom system and associated control opens the door to smaller, more efficient, and more reliable reactive power compensators.

REFERENCES

[1] J. S. Lai and F. Z. Peng, "Multilevel converters-a new breed of power converters," *IEEE Trans. Ind. Appl.*, vol. 32, no. 3, pp. 509–517, May/Jun. 1996.

[2] F. Z. Peng, J. S. Lai, J. W. McKeever, and J. VanCoevering, "A multilevel voltage-source inverter with separate DC sources for static VAr generation," *IEEE Trans. Ind. Appl.*, vol. 32, no. 5, pp. 1130–1138, Sep./Oct. 1996.

[3] Y. Liang and C. O. Nwankpa, "A new type of StatCom based on cascading voltage-source inverters with phase-shifted unipolar SPWM," *IEEE Trans. Ind. Appl.*, vol. 35, no. 5, pp. 1118–1123, Sep./Oct. 1999.

[4] Y. Neyshabouri, H. Iman-Eini, and M. Miranbeigi, "State feedback control strategy and voltage balancing scheme for a transformer-less STATic synchronous COMpensator based on cascaded H-bridge converter," *IET Power Electron*., vol. 8, no. 6, pp. 906–917, Jun. 2015.

[5] L. K. Haw, M. S. A. Dahidah, and H. A. F. Almurib, "A new reactive current reference algorithm for the STATCOM system based on cascaded multilevel inverters," *IEEE Trans. Power Electron.*, vol. 30, no. 7, pp. 3577–3588, Jul. 2015.

[6] L. K. Haw, M. S. A. Dahidah, and H. A. F. Almurib, "SHE–PWM cascaded multilevel inverter with adjustable DC voltage levels control for STATCOM applications," *IEEE Trans. Power Electron.*, vol. 29, no. 12, pp. 6433–6444, Dec. 2014.

[7] C. D. Townsend, T. J. Summers, and R. E. Betz, "Impact of practical issues on the harmonic performance of phase-shifted modulation strategies for a cascaded H-bridge StatCom," *IEEE Trans. Ind. Electron.*, vol. 61, no. 6, pp. 2655–2664, Jun. 2014.

[8] C.-T. Lee *et al.*, "Average power balancing control of a STATCOM based on the cascaded H-bridge PWM converter with star configuration," *IEEE Trans. Ind. Appl.*, vol. 50, no. 6, pp. 3893–3901, Nov./Dec. 2014.

[9] R. Xu, Y. Yu, R. Yang, G. Wang, D. Xu, B. Li, and S. Sui, "A novel control method for transformerless H-bridge cascaded StatCom with star configuration," *IEEE Trans. Power Electron.*, vol. 30, no. 3, pp. 1189–1202, Mar. 2015.

[10] H. Akagi, S. Inoue, and T. Yoshii, "Control and performance of a transformerless cascade PWM StatCom with star configuration," *IEEE Trans. Ind. Appl.*, vol. 43, no. 4, pp. 1041–1049, Jul.-Aug. 2007.

[11] K. Fujii and R. W. De Doncker, "A novel DC-link voltage control of PWM-switched cascade cell multi-level inverter applied to StatCom," in *Proc. 40th IAS Annual Meet.*, Oct. 2005, vol. 2, pp. 961–967.

[12] J. de Leon Morales, M. F. Escalante, and M. T. Mata-Jimenez, "Observer for dc voltages in a cascaded H-bridge multilevel StatCom," *IET Elect. Power Appl.*, vol. 1, no. 6, pp. 879–889, Nov. 2007.

[13] L. Yidan and B. Wu, "A novel dc voltage detection technique in the CHB inverter-based StatCom," *IEEE Trans. Power Del.*, vol. 23, no. 3, pp. 1613–1619, Jul. 2008.

[14] J. A. Barrena, L. Marroyo, M. A. R. Vidal, and J. R. T. Apraiz, "Individual voltage balancing strategy for PWM cascaded H-bridge converter-based StatCom," *IEEE Trans. Ind. Electron.*, vol. 55, no. 1, pp. 21–29, Jan. 2008.

[15] C. Han, A. Q. Huang, Y. Liu, and B. Chen, "A generalized control strategy of per-phase DC voltage balancing for cascaded multilevel converter-based StatCom," in *Proc. IEEE PESC*, Jun. 17–21, 2007, pp. 1746–1752.

[16] W. Song and A. Q. Huang, "Fault-tolerant design and control strategy for cascaded H-bridge multilevel converter-based StatCom," *IEEE Trans. Ind. Electron.*, vol. 57, no. 8, pp. 2700–2708, Aug. 2010.

[17] Y. Liu, A. Q. Huang, W. Song, S. Bhattacharya, and G. Tan, "Small-signal model-based control strategy for balancing individual DC capacitor voltages in cascade multilevel inverter-based StatCom," *IEEE Trans. Ind. Electron.*, vol. 56, no. 6, pp. 2259–2269, Jun. 2009.

[18] N. Hatano and T. Ise, "Control scheme of cascaded H-bridge StatCom using zero-sequence voltage and negative-sequence current," *IEEE Trans. Power Del.*, vol. 25, no. 2, pp. 543–550, Apr. 2010.

[19] C. D. Townsend, T. J. Summers, and R. E. Betz, "Multigoal heuristic model predictive control technique applied to a cascaded H-bridge StatCom," *IEEE Trans. Power Electron.*, vol. 27, no. 3, pp. 1191–1200, Mar. 2012.

[20] C. D. Townsend, T. J. Summers, J. Vodden, A. J. Watson, R. E. Betz, and J. C. Clare, "Optimization of switching losses and capacitor voltage ripple using model predictive control of a cascaded H-bridge multilevel StatCom," *IEEE Trans. Power Electron.*, vol. 28, no. 7, pp. 3077–3087, Jul. 2013.

[21] K. Sano and M. Takasaki, "A transformerless D-StatCom based on a multivoltage cascade converter requiring no DC sources," *IEEE Trans. Power Electron.*, vol. 27, no. 6, pp. 2783–2795, Jun. 2012.

[22] S. Du, J. Liu, J. Lin, and Y. He, "A novel DC voltage control method for StatCom based on hybrid multilevel H-bridge converter," *IEEE Trans. Power Electron.*, vol. 28, no. 1, pp. 101–111, Jan. 2013.

[23] B. Gultekin and M. Ermis, "Cascaded multilevel converter-based transmission StatCom: system design methodology and development of a 12 kV $\pm$ 12 MVAr power stage," *IEEE Trans. Power Electron.*, vol. 28, no. 11, pp. 4930–4950, Nov. 2013.

[24] C. D. Townsend, T. J. Summers, and R. E. Betz, " Issues on the harmonic performance of phase-shifted modulation strategies for a cascaded H-bridge StatCom," *IEEE Trans. Ind. Electron.*, vol. 61, no. 6, pp. 2655–2664, Jun. 2014.

[25] H. Wang, M. Liserre, and F. Blaabjerg, "Toward reliable power electronics—challenges, design tools and opportunities," *IEEE Ind. Electron. Mag.*, vol. 7, no. 2, pp. 17–26, Jun. 2013.

[26] S. Yang *et al.*, "An industry-based survey of reliability in power electronic converters," *IEEE Trans. Ind. Appl.*, vol. 47, no. 3, pp. 1441–1451, May/Jun. 2011.

[27] B. Karanayil, V. G. Agelidis, and J. Pou, "Evaluation of DC-link decoupling using electrolytic or polypropylene film capacitors in three-phase grid-connected photovoltaic inverters," in *Proc. 39th Annu. Conf. IEEE Ind. Electron. Soc.*, Nov. 10–13, 2013, pp. 6980–6986.

[28] H. Wang and F. Blaabjerg, "Reliability of capacitors for DC-link applications in power electronic converters – An overview," *IEEE Trans. Ind. Appl.*, vol. 50, no. 5, pp. 3569–3578, Sep./Oct. 2014.

[29] H. R. Andersen, R. Tan, and C. Kun, "3-phase AC-drives with passive front-ends with focus on the slim DC-link topology," in *Proc. IEEE PESC*, Jun. 15–19, 2008, pp. 3248–3254.

[30] R. Maheshwari, S. Munk-Nielsen, and S. Busquets-Monge, "Design of neutral-point voltage controller of a three-level NPC inverter with small DC-link capacitors," *IEEE Trans. Ind. Electron.*, vol. 60, no. 5, pp. 1861–1871, May 2013.

[31] B. Gültekin, "Cascaded multilevel converter based transmission StatCom: System design methodology and development of a 12 kv $\pm$ 12 MVAR power-stage", Ph.D. dissertation, Dept. Elect. Eng., Middle East Technical Univ., Ankara, Turkey, 2012.

[32] H. R. Zeller, "Cosmic ray induced failures in high power semiconductor devices," *Microelectron. Reliability*, vol. 37, no. 10–11, pp. 1711–1718, Oct./Nov. 1997.

[33] D. G. Holmes and D. A. Martin, "Implementation of a direct digital predictive current controller for single and three phase voltage source inverters," in *Proc. IEEE 31st IAS Annu. Meeting Ind. Appl. Conf.*, Oct. 1996, vol. 2, pp. 906–913.

[34] R. Betz, B. Cook, and S. Henriksen, "A digital current controller for three phase voltage source inverters," in *Proc. IEEE 32nd IAS Annu. Meeting Ind. Appl. Conf.*, Oct. 1997, pp. 722–729.

[35] S. Kouro, P. Lezana, M. Angulo, and J. Rodriguez, "Multicarrier PWM with dc-link ripple feedforward compensation for multilevel inverters," *IEEE Trans. Power Electron.*, vol. 23, no. 1, pp. 52–59, Jan. 2008.

[36] G. Farivar, B. Hredzak, and V. G. Agelidis, "Reduced capacitance thin-film H-bridge multilevel StatCom control utilizing an analytic filtering scheme," *IEEE Trans. Ind. Electron.*, vol. 62, no. 10, pp. 6457–6468, Oct. 2015.

[37] G. Farivar, B. Hredzak, and V. G. Agelidis, "Decoupled control system for cascaded H-bridge multilevel converter based StatCom," *IEEE Trans. Ind. Electron.*, vol. 63, no. 1, pp. 322–331, Jan. 2016.
[38] P. Voss *et al.*, "Irradiation experiments with high-voltage power devices as a possible means to predict failure rates due to cosmic rays," in *Proc. IEEE Int. Symp. Power Semiconductor Dev. IC's*, May 26–29, 1997, pp. 169–172.
[39] T. Shoji *et al.*, "Neutron induced single-event burnout of IGBT," in *Proc. Int. Power Electron. Conf.*, Jun. 21–24, 2010, pp. 142–148.
[40] F. Bauer, N. Kaminski, S. Linder, and H. Zeller, "A high voltage IGBT and diode chip set designed for the 2.8 kV DC link level with short circuit capability extending to the maximum blocking voltage," in *Proc. 12th Int. Symp. Power Semiconductor Dev. ICs*, 2000, pp. 29–32.

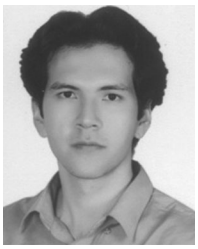

Ghias Farivar (S'13) received the B.Sc. degree in electrical engineering from Nooshirvani Institute of Technology, Babol, Iran, in 2008, and the M.Sc. degree in power electronics from the University of Tehran, Tehran, Iran in 2011.

He is currently working toward the Ph.D. degree at the Australian Energy Research Institute, University of New South Wales, Sydney, N.S.W., Australia. His research interests include renewable energy systems, power convertors, FACTS devices, and hybrid electric vehicles.

Christopher David Townsend (S'09-M'13) received the B.E. and Ph.D. degrees, in 2009 and 2013, respectively, in electrical engineering from the University of Newcastle, Newcastle, N.S.W., Australia.

Between 2012 and 2016, he spent four years with both ABB Corporate Research, Västerås, Sweden and Australian Energy Research Institute, University of New South Wales, Sydney, N.S.W. He is currently a Postdoctoral Researcher at the University of Newcastle, Australia. His current research interests include topologies and modulation strategies for multilevel converters.

Dr. Townsend is a member of the Power Electronics and Industrial Electronics Societies of the IEEE.

Branislav Hredzak (M'98-SM'13) received the B.Sc. and M.Sc. degrees from the Technical University of Kosice, Kosice, Slovak Republic, in 1993, and the Ph.D. degree from Napier University of Edinburgh, Edinburgh, U.K., in 1997, all in electrical engineering.

He was as a Lecturer and a Senior Researcher in Singapore from 1997 to 2007. He is currently a Senior Lecturer in the School of Electrical Engineering and Telecommunications, University of New South Wales, Sydney, N.S.W., Australia. His current research interests include hybrid storage technologies and advanced control systems for power electronics and storage systems.

Josep Pou (S'97–M'03–SM'13) received the B.S., M.S., and Ph.D. degrees in electrical engineering from the Technical University of Catalonia (UPC), Catalonia, Spain, in 1989, 1996, and 2002, respectively.

In 1990, he joined the faculty of UPC as an Assistant Professor, where he became an Associate Professor in 1993. Since February 2013, he has been a Professor with the University of New South Wales (UNSW), Sydney, N.S.W., Australia. From February 2001 to January 2002, and February 2005 to January 2006, he was a Researcher at the Center for Power Electronics Systems, Virginia Tech, Blacksburg, VA, USA. From January 2012 to January 2013, he was a Researcher at the Australian Energy Research Institute, UNSW. Since 2006, he has been collaborated with TECNALIA Research & Innovation as a research consultant. He has authored more than 200 published technical papers and has been involved in several industrial projects and educational programs in the fields of power electronics and systems. His research interests include modulation and control of power converters, multilevel converters, renewable energy generation, energy storage, power quality, and HVDC transmission systems.

Vassilios G. Agelidis (S'89-M'91-SM'00-F'16) was born in Serres, Greece. He received the B.Eng. degree in electrical engineering from the Democritus University of Thrace, Thrace, Greece, in 1988, the M.S. degree in applied science from Concordia University, Montreal, QC, Canada, in 1992, and the Ph.D. degree in electrical engineering from Curtin University, Perth, W.A., Australia, in 1997.

He was with Curtin University (1993–1999); the University of Glasgow, Glasgow, U.K. (2000–2004); Murdoch University, Perth, Australia (2005–2006); and the University of Sydney, Sydney, N.S.W., Australia (2007–2010). He is currently the Director in the Australian Energy Research Institute, School of Electrical Engineering and Telecommunications, University of New South Wales (UNSW), Sydney, N.S.W., Australia.

Dr. Agelidis received the Advanced Research Fellowship from the U.K.'s Engineering and Physical Sciences Research Council in 2004. He was the Vice President for Operations with the IEEE Power Electronics Society from 2006 to 2007. He was an AdCom Member of the IEEE PELS from 2007 to 2009 and the Technical Chair of the 39th IEEE Power Electronics Specialists Conference in 2008 held in Rhodes, Greece.